Journal of Soil Contamination, 2(1): (1993)

The Effect of Soil-Particle Size on Hydrocarbon Entrapment Near a Dynamic Water Table

Robert G. Ryan and V. K. Dhir

Department of Mechanical, Aerospace, and Nuclear Engineering, University of California, Los Angeles, CA 90024

ABSTRACT: The entrapment of residual hydrocarbon globules by water table fluctuations can produce a long-term contamination threat to groundwater supplies that is difficult to remove. The mobilization of entrapped hydrocarbon globules depends on the balance between capillary and gravitational forces represented by the Bond number. It is important to estimate the potential for hydrocarbon entrapment at a spill site due to its influence on the effectiveness of remediation efforts. The present work focuses on the influence of particle diameter on hydrocarbon entrapment for a typical LNAPL (light nonaqueous-phase liquid). Laboratory column tests have been conducted using a dual-beam gamma densitometer to measure saturations of the three phases (water, air, and hydrocarbon). Soltrol 170®, a solvent manufactured by Phillips 66 Co., is used as the hydrocarbon. Residual saturation of the Soltrol is measured after fluctuations in water table level to establish the distribution and consistency of hydrocarbon entrapment below the water table. Glass particles of nearly uniform size were used to represent a sandy soil. In the experiments, average particle sizes ranged from 210 to 6000 μm. Data were also taken using the synthetic soil matrix approved by the U.S. Environmental Protection Agency (EPA) for contamination studies. Results show that the distribution of trapped LNAPL is quite uniform and that the average residual saturation is about 13% up to a particle diameter of 710 μm. Above this diameter, residual saturation decreases with particle size. The corresponding critical Bond number, determined experimentally, agrees well with the predicted value of 1.6.

KEY WORDS: petroleum hydrocarbons, groundwater contamination, soil contamination.

I. INTRODUCTION

Petroleum products and organic solvents present in a soil matrix can become a significant source of groundwater contamination. These contaminants are referred to as nonaqueous-phase liquids (NAPLs) because they are generally immiscible with water. NAPLs are further subdivided into LNAPLs and DNAPLs, depending on whether the contaminant is lighter or denser, respectively, than water.

If the contaminant is LNAPL and the spill is of sufficient size, the plume will migrate laterally when it reaches the water table. During the early part of the lateral movement, the LNAPL displaces water underneath the source location, locally depressing the water table as shown in Figure 1. Eventually the plume will spread out laterally over the capillary fringe, and the local water table level will recover. A region of entrapped LNAPL at residual saturation will be present in the region from which the water table was temporarily displaced. In addition, the lateral spreading is influenced by the seasonal fluctuations of the water table, which vertically displace the free LNAPL near the capillary fringe. The vertical displacement produces a zone of LNAPL at residual saturation levels; the thickness of the zone is directly related to the amplitude of the water table movement. This zone has been described as an "immiscible lens" of water and contaminant (Faust, 1985).

The displacement of LNAPL by a dynamic water table is a special case of static distribution of fluids in porous media. The classic work relating saturation to capillary pressure was done by Leverett (1941). Experiments were performed on clean sands with water and air as the fluids in both the imbibition and the drainage modes. The effect of hysteresis on the relationship was clearly shown.

More recent efforts include those of Lenhard and Parker (1988). A three-phase retention cell was developed so that the pressures of the water and

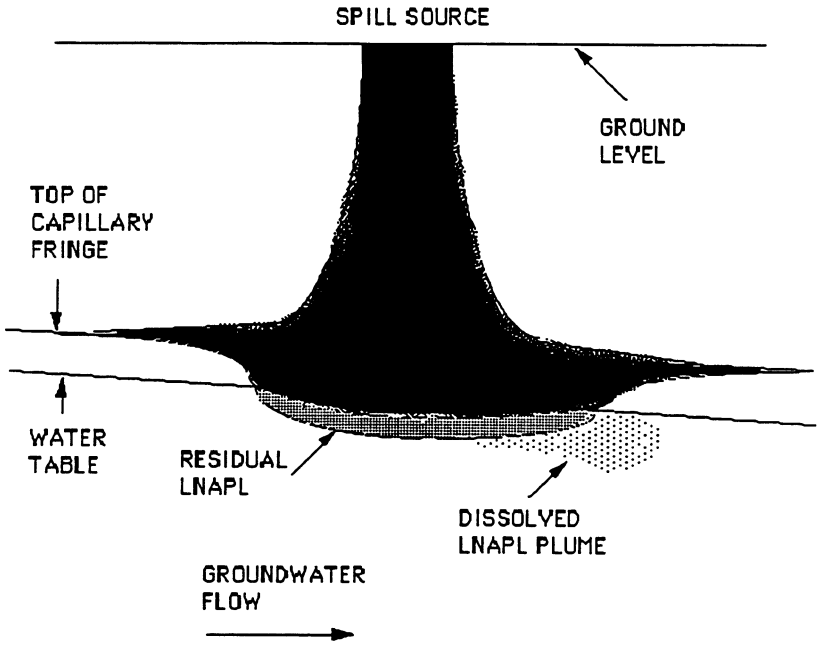

FIGURE 1. Interaction of LNAPL spill with water table.

contaminant phases could be simultaneously measured. Their results indicated that Leverett's correlation could be extended to three components, with the assumption that the order of wettability was water, LNAPL, air. Parker and Lenhard (1987) noted the complexity of hysteresis in three-component systems due to the greater number of possible path directions. Their model used water-air drainage saturation data to develop a pore-size distribution for the medium, based on fitted parameters describing the saturation profile. Using these parameters and two-component residual saturation data, three-component saturation profiles were predicted for any path direction. The LNAPL phase was assumed to exist continuously ("free" LNAPL) or as discontinuous globules or ganglia ("trapped" LNAPL). Numerical simulations of LNAPL entrapment due to water table fluctuations were presented in Lenhard, Parker, and Kaluarachchi (1989).

Hunt, Sitar, and Udell (1988) reviewed the physical mechanisms for LNAPL transport. From simplified force balances on LNAPL ganglia, they showed that a rising water table can trap LNAPL ganglia below the water table level. Relationships were derived for the maximum vertical height of stable ganglia in the saturated zone and in the unsaturated zone. For hydrocarbons, the maximum stable ganglion length in the saturated zone was longer than it was in the unsaturated zone. Thus the authors concluded that a rising water table would not displace ganglia formed in the unsaturated zone.

The effect of contaminant distribution in the capillary fringe and saturated zones on groundwater remediation efforts has been well described by Hoag, Marley, Cliff, and Nangeroni (1991). Others, such as Baehr (1987), have noted the role of the capillary fringe zone as a barrier to aquifer contamination. The amount and distribution of the contaminant that does reach the saturated zone determine the interfacial area between the LNAPL and water phases and the subsequent mass-transfer rate of the contaminant. Imhoff, Jaffe, and Pinder (1990) found a dependence of mass-transfer coefficient on residual saturation using TCE (a DNAPL) as the contaminant, although it is probable that other parameters are also important.

Many papers have been published on the subject of mobilizing residual amounts of oil by waterflooding. It has generally been noted that significant mobilization of the residual ganglia occurs at a critical value of the capillary number. The capillary number can be expressed as

$$N_{ca} = k\Delta P / L\sigma$$

where k = permeability of the porous medium, $\Delta P/L$ = viscous pressure gradient, and σ = interfacial tension.

Experimentally, the critical value of capillary number for ganglia mobilization has been found by various researchers to be about 1E-3. Observations by Wardlaw and McKellar (1985) indicate that the larger ganglia break up upon mobilization, so that there is no significant movement of the nonwetting phase until the capillary

number is high enough to mobilize single pore blobs, or singlets. They concluded that the capillary number of 1E-3 corresponds to singlet mobilization.

Boyd and Farley (1992) assessed the possibility of DNAPL removal using alcohol flooding by measuring TCE removal from columns of glass bead packs and representative South Carolina soil. Their results are consistent with the earlier oil recovery findings. The data are correlated using a mobility number that includes the effect of both capillary number and Bond number. Mobilization of entrapped TCE began at a mobility number of 1E-4, whereas complete removal was achieved at 1E-2.

The goal of the present work is to study the factors that influence the residual LNAPL contaminant saturation near a slowly changing water table. Particle size is varied to assess the impact of the balance between gravitational and buoyancy forces on LNAPL entrapment. The use of a dual-beam gamma densitometer to measure *in situ* LNAPL saturation allows the amount and spatial distribution of the residual LNAPL to be evaluated after each water table fluctuation.

II. ESTIMATION OF CRITICAL BOND NUMBER

The difficulties encountered in the complete description of distribution of fluids in porous media can be minimized by considering specific conditions that are important to the prediction of aquifer contamination levels. The most dangerous LNAPL in terms of its contamination potential is the residual amounts that are trapped in the saturated zone during water table fluctuations. The residual LNAPL is in the form of discontinuous ganglia that may remain trapped, depending on the balance between buoyancy and capillary forces. The difficulty in describing the pore space geometry in a porous medium such as soil suggests the use of a simplified geometry to identify the important physical parameters.

Oh and Slattery (1979) used a periodically constricted tube to model the pore space, as shown in Figure 2. Calculations were performed to estimate the pressure difference required to move an oil ganglion through the pore as a function of bulge radius, ganglion volume, and contact angle. The required pressure difference varies periodically as the ganglion changes position; the calculated maximum value was taken to be the pressure difference required for mobilization. The mobilizing pressure difference was found to be a periodic function of ganglion volume. By varying ganglion volume over one period, the range of values for the mobilizing pressure difference (assuming water-wet conditions) was

$$0.323 \leq (\Delta \mathrm{Pr}_n / 2\sigma)_{mob} \leq 0.884 \tag{1}$$

where r_n = neck radius of the pore and ΔP = pressure difference across the ganglion.

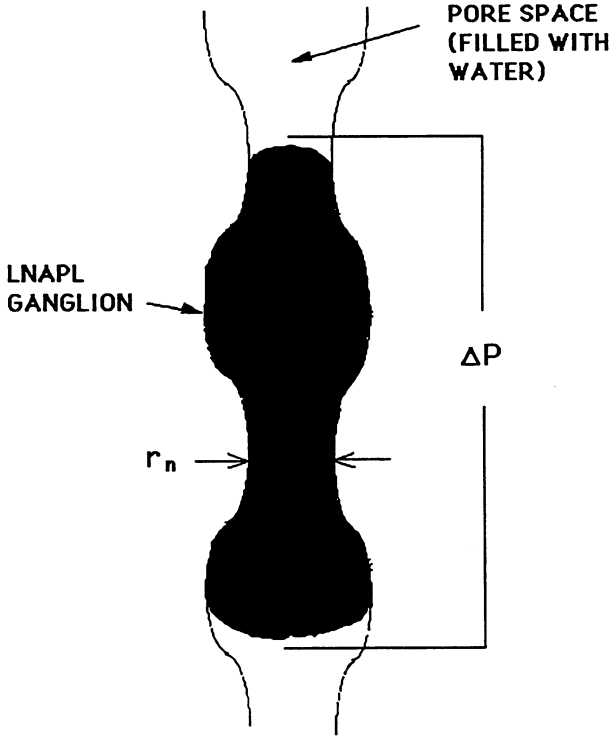

FIGURE 2. Trapped LNAPL ganglion in model pore space.

The effect of the neck radius and the interfacial tension on the mobilizing pressure difference is clearly shown. For the oil-wet case, similar calculations gave

$$0.557 \le (\Delta P r_n / 2\sigma)_{mob} \le 0.979$$

which indicates that displacement is somewhat more difficult under these conditions.

For a ganglion trapped under the water table, the unbalanced hydrostatic pressure gradient ($\Delta P/L$) is $\Delta\rho g$. Assuming that the assertion of Wardlaw and McKellar (1985) is correct regarding the necessity of mobilizing single pore blobs, then L is approximately equal to the particle diameter (D_p). If it is also assumed that the neck radius can be expressed as a constant B times the particle diameter, then

$$\Delta P r_n / 2\sigma = B\Delta\rho g D_p^2 / 2\sigma$$

Mason (1971) calculated pore-size distributions in random packings of equal spheres. According to these results, the possible range for constant B is from 0.075

to 0.3, with the largest number of pores at the lower extreme. A value of 0.075 is used here. Substituting these results back into Equation 1 gives

$$8.6 \le \mathrm{Bo}_{\mathrm{crit}} \le 23.6$$

where Bo = Bond number = $gD_p^2\Delta\rho/\sigma$

The Bond number represents the ratio of the buoyancy forces to the capillary forces. The critical value of Bond number corresponds to the pressure difference required for mobilizing single pore blobs, assuming water-wet conditions.

Another estimate for the critical Bond number can be obtained from the value of critical capillary number for oil displacement by waterflooding. The key assumption is that the hydrostatic pressure gradient acting on the LNAPL ganglia behaves in a similar way to the viscous pressure gradient present in waterflooding at high capillary numbers.

From the results of Wardlaw and McKeller (1985), the critical capillary number may be written as

$$k\Delta P / L\sigma \approx 1E-3 \qquad (2)$$

The permeability of a medium of spherical particles can be evaluated from an empirical correlation (Bear, 1972) as

$$k = 6.17E-4D_p^2$$

Once again the hydrostatic pressure gradient is $\Delta\rho g$. Making these substitutions in Equation 2 yields

$$\mathrm{Bo}_{\mathrm{crit}} \approx 1E-3/6.17E-4 = 1.6$$

The result is a critical Bond number of 1.6. Recalling the relationship between the critical capillary number and the mobilization of single pore blobs, the conclusion is that a Bond number of 1.6 corresponds to the mobilization of singlets due to buoyancy. This estimate is somewhat lower than the range derived from the work of Oh and Slattery (1979).

It is not immediately clear whether residual saturation should vary continuously with Bond number, or whether a discontinuous change associated with the critical value is to be expected. The size and distribution of the LNAPL ganglia created during the displacement process may be influenced by any number of factors, including the pore-size distribution. The existence of a critical Bond number for glass bead packings is examined experimentally by testing particle diameters from 210 to 600 μm.

III. EXPERIMENTAL METHODS

A test section for LNAPL displacement measurements was constructed from a 9-in-long segment of 3-in-inner-diameter Plexiglas® tubing. Several probes were placed in the tubing wall to allow air to escape during the LNAPL infiltration process, thus simulating a medium that was unconfined in the horizontal direction. A fine stainless steel screen was used at the top and bottom of the test section to hold the porous material in place. The bottom of the test section was connected to a supply tank used to control the water table height. Gamma attenuation measurements were taken at six points along the test section to establish liquid saturations. Details of the test section are shown in Figure 3 and Table 1.

Obtaining three-component (water, LNAPL, and air) saturation data is far more difficult than two-component data. The instrument used in this study was a dual-beam gamma densitometer. The first gamma densitometry in soil analysis used a single monoenergetic beam (Ferguson and Gardner, 1962). A single beam was sufficient for measuring water content in a nonswelling medium. To extend the

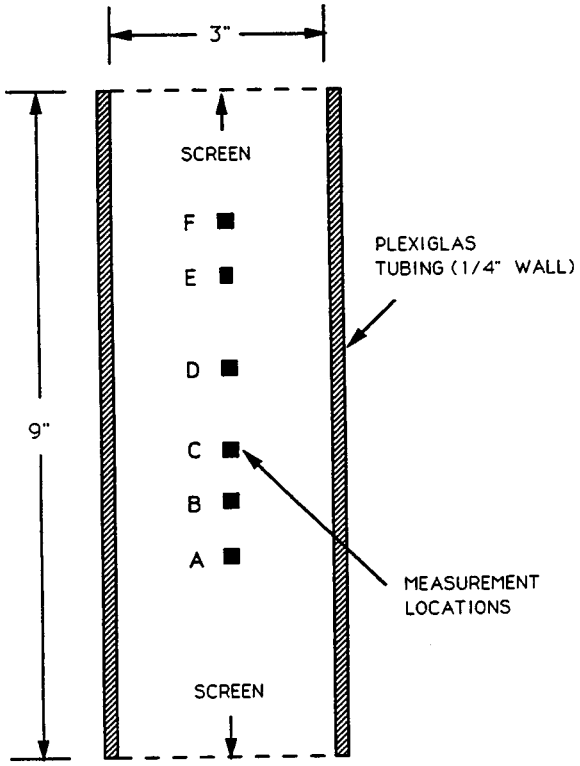

FIGURE 3. Schematic of test section.

TABLE 1
Test Section Measurement Location

Measurement location	Height from bottom of column (in.)
A[a]	2.7
B	3.4
C	4.1
D	5.2
E	6.5
F	7.2

[a] See Figure 3 for corresponding locations.

method to a medium with changing bulk density, a dual-energy beam was required. Although not the first to use this method, Nofziger and Swartzendruber (1974) refined the experimental setup and calibration procedures. The two sources were americium (60 keV) and cesium (662 keV). Ferrand, Milly, and Pinder (1986) extended the dual-beam technique to three-component systems in nonswelling media. The degree of saturation cannot be found from their approach because the porosity was not evaluated as part of the calibration procedure.

Lenhard et al. (1988) used the dual-beam technique for transient experiments using Soltrol 170® (a hydrocarbon solvent manufactured by the Phillips Chemical Co.) as the contaminant. To improve accuracy, the water and Soltrol 170 were "doped" with sodium bromide and iodoheptane to enhance the differences in attenuation coefficients. The measured values of fluid content were converted to saturations by using a porosity based on bulk soil density measurements.

The calibration procedure used by Lenhard et al. (1988) is modified here to allow for the determination of local porosity based on attenuation measurements. The fundamental law governing attenuation of gamma radiation through a medium is given as

$$I = I_o \exp(-\mu X)$$

where I = count rate of the attenuated beam, I_o = count rate with no attenuation, μ = linear attenuation coefficient, and X = thickness of the medium. The attenuation coefficient μ is a function of the gamma beam energy.

If the attenuation coefficient of the solid material in the porous medium is known, the gamma attenuation through the dry medium can be used to find porosity. First, the count rate I_o through the empty test section is measured. After filling the test section with the porous medium and measuring the attenuated count rate I, the attenuation relation can be written as

$$I = I_o \exp(-\mu_s X(1-\varepsilon))$$

where μ_s = attenuation coefficient for solid material and ε = porosity. Thus the porosity can be found at each measurement point i from

$$\varepsilon_i 1 - \left[\ln\left(I_o / I\right)_i\right] \Big/ \left(\mu_s X_i\right) \tag{3}$$

Because the porosity can be calculated from a single beam, the second beam is used as a cross-check.

For a nonswelling porous medium saturated by two liquids and air, where the subscripts a and c refer to the two gamma energies and the subscripts 1 and 2 denote the two liquids, the result is

$$I_a = I_{oa} \exp\left(-\mu_{a1} X S_1 \varepsilon - \mu_{a2} X S_2 \varepsilon\right)$$
$$I_c = I_{oc} \exp\left(-\mu_{c1} X S_1 \varepsilon - \mu_{c2} X S_2 \varepsilon\right)$$

where I = count rate through the saturated medium, I_o = count rate through the dry medium, and S = liquid saturation. Rearranging yields the following relations:

$$\mu_{a1} S_1 + \mu_{a2} S_2 = \ln\left(I_{oa} / I_a\right) \Big/ \varepsilon L = C_a$$
$$\mu_{c1} S_1 + \mu_{c2} S_2 = \ln\left(I_{oc} / I_c\right) \Big/ \varepsilon L = C_c$$

Putting the equations in matrix form gives

$$\begin{vmatrix} \mu_{a1} & \mu_{a2} \\ \mu_{c1} & \mu_{c2} \end{vmatrix} \begin{vmatrix} S_1 \\ S_2 \end{vmatrix} = \begin{vmatrix} C_a \\ C_c \end{vmatrix}$$

or

$$\mathbf{AS} = \mathbf{C} \tag{4}$$

Thus the liquid saturations can be found from

$$\begin{vmatrix} S_1 \\ S_2 \end{vmatrix} \begin{vmatrix} \mu_{a1} & \mu_{a2} \\ \mu_{c1} & \mu_{c2} \end{vmatrix}^{-1} \begin{vmatrix} C_a \\ C_c \end{vmatrix}$$

or

$$\mathbf{S} = \mathbf{A^{-1}C} \tag{5}$$

The air saturation (S_3) can be found from

$$S_3 = 1 - \left(S_1 + S_2\right) \tag{6}$$

The experimental uncertainty in determining the liquid saturations is divided into "calibration uncertainty" and "measurement uncertainty." The calibration uncertainty is a result of the uncertainties in the elements of the inverse of the coefficient matrix **A**, which depend on the uncertainties in the liquid attenuation coefficients. If the coefficient matrix is "ill conditioned," the calibration uncertainty becomes untenable. The attenuation properties of water and light hydrocarbons are such that the coefficient matrix is normally ill conditioned. Following the method of Lenhard et al. (1988), sodium bromide and iodoheptane are used as doping agents, and the calibration uncertainty is sufficiently reduced. The measurement uncertainty is a function of the uncertainty in the elements of the **C** matrix, which depends on attenuation measurements through the test section during each run. The uncertainties of the measured count rates are based on the square root of the count rate because radioactive decay behaves as a Poisson distribution.

The attenuation coefficients are found experimentally using a rectangular test box that is partitioned into four compartments. Measurements are taken of gamma attenuation as the compartments are sequentially filled with liquid or dry porous material. Again the count rate I_o represents the count rate through the empty box. The relations for the liquids and the glass particles (and soils) are

$$\mu_l = \ln\left(I_o / I_N\right) \Big/ X_N \text{ (liquids)} \tag{7}$$

$$\mu_s = \ln\left(I_o / I_N\right) \Big/ X_N\left(1-\varepsilon_N\right) \text{ (porous material)} \tag{8}$$

where N = the number of compartments filled and

$$X_N - \sum_{i=1}^{N} X_i$$

Linear regression is used with Equations 7 and 8 to find the attenuation coefficients and their uncertainties. For the glass particles and soils, the porosity in the test box (ε_i) is determined gravimetrically. The high degree of linearity found for the solid materials confirms the reliability of this technique.

The dual-beam densitometer was built by modifying an existing single beam densitometer fitted with a cesium source. Modification of the existing source collimator was required to accommodate the addition of an americium source located in the University of California at Los Angeles (UCLA) inventory. A brass holder was designed to mount to the existing source collimator and place the americium source in front of the cesium source. A steel collimator slides into a 1-in. hole in the brass holder in front of the americium source to give a

rectangular beam with a vertical thickness of 1/8 in. A sodium iodide detector is mounted behind a lead collimator with a 1/8 × 1.25-in. slot to capture the attenuated beam. The use of a rectangular beam allows shorter count durations and better averaging at each vertical location. The total counts at the two gamma energies are integrated with a Tracor-Northern® TN-7200 multichannel analyzer. A schematic of the densitometer arrangement is shown in Figure 4.

Because the beam is a thin fan-shaped beam, the path length through the attenuating material is not the same for each photon. The path length variation is also dependent on the geometry of the attenuating medium and the location of the gamma source. A path length correction factor was found for both beams by numerically integrating over the possible path lengths. The correction factor was used to correct the lengths in Equations 3, 5, 7, and 8. The values of the correction factors for the americium and cesium beams were 1.000084 and 1.000058, respectively, for the test box geometry and 0.998442 and 0.998156, respectively, for the test section geometry.

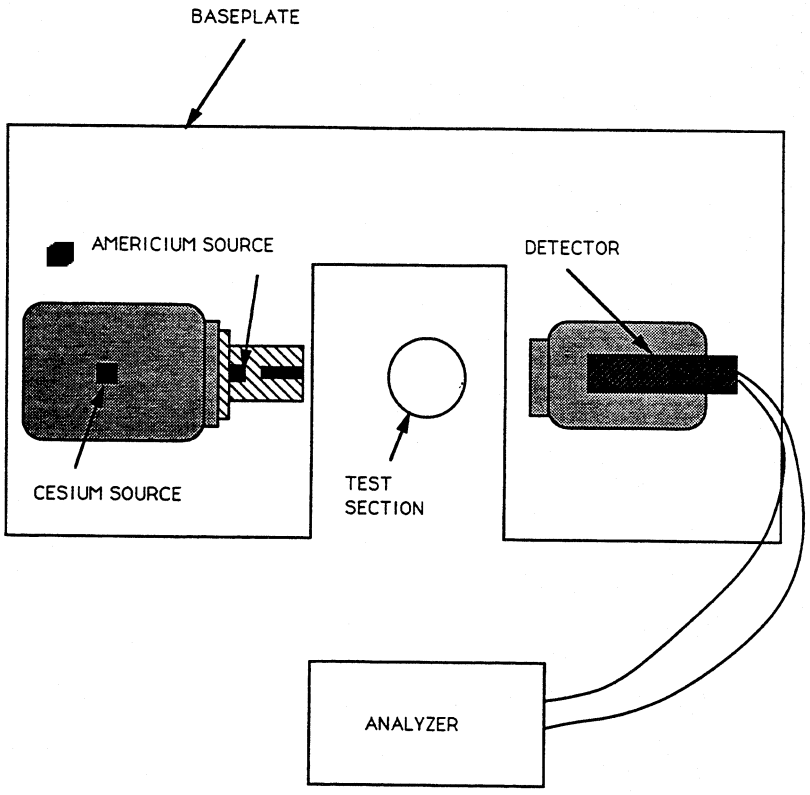

FIGURE 4. Densitometer schematic.

A plenum at the bottom of the test section is connected to a reservoir containing the sodium bromide solution. The height of the reservoir can be adjusted to simulate change in the water table height. A rotameter is installed in the connecting tubing to allow for flow rate measurement. Above the test section is a section of clear Plexiglas tubing so the layer of displaced LNAPL can be observed. Figure 5 shows the arrangement of the apparatus.

A series of runs was conducted using six sizes of glass particles and a standard test soil. The procedure for each run consisted of several steps to simulate the effect of water table movement on the LNAPL sitting above the water table. First, the gamma attenuation through the empty test section was recorded at the six measurement points. Next, the test section was filled with the porous material while the column assembly was vibrated to allow for even packing. Attenuation measurements through the dry medium were made to establish the porosity at each point, using Equation 3.

The sodium bromide solution in the reservoir (subsequently referred to as "water") consisted of 75 g of sodium bromide per 1000 cm^3 of distilled water. The solution was allowed to fill the test section from the bottom until the visible interface between the wet and dry portions was approximately two thirds of the way through the column. The flow was then halted and a sufficient amount was drained from the test section so that only the bottom portion of the test section was fully saturated. Note that because the shutoff valve between the supply tank and the test section remained closed after the water was introduced, this method did not provide an equilibrium drainage saturation profile. This procedure provided a

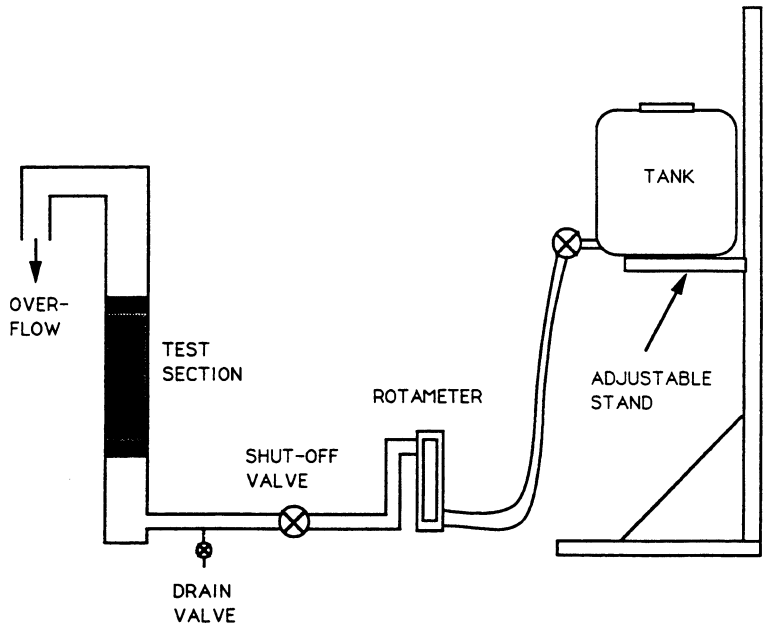

FIGURE 5. Test apparatus schematic.

consistent initial saturation profile that was nearly independent of particle diameter, allowing the comparison of water-wet and dry regions in the unsaturated zone in a relatively short test section. The initial water saturation profile was measured by taking attenuation measurements through the test section. For this case only a single beam was needed; the data from the second beam were used as a cross-check.

After the initial water profile was established, 200 cm^3 of the 9:1 mixture of Soltrol 170 and iodoheptane (subsequently referred to as "LNAPL") was added to the top of the column. As the LNAPL infiltrated the test section, air was allowed to escape through the probes in the test section wall. After equilibrium was reestablished, another gamma scan was taken to establish the saturation profiles of the LNAPL and water. Subsequently water was slowly introduced at the bottom of the test section, displacing the LNAPL upward. Eventually a free LNAPL layer appeared above the test section exit, and a gamma scan of the test section established the new saturation profiles. The thickness of the free LNAPL layer was measured to establish the total displaced volume. Approximately 100 cm^3 of this layer was drained off so that the LNAPL attenuation coefficient could be measured in the test box, but it was reintroduced at the top of the column before the run was completed.

One more cycle of lowering and then raising the water table height was performed to complete each run. During the lowering of the water table, the LNAPL that previously was displaced from the test section was allowed to reinfiltrate the column. The reinfiltration was to establish the maximum retention of trapped LNAPL in repeated displacements. Also, a sufficient amount of water was withdrawn to provide a sample for attenuation coefficient measurement. The saturation profiles were measured before and after the second displacement.

The water flow rates used during the LNAPL displacements were kept sufficiently low to avoid viscous and inertial effects. The maximum Reynolds number for any run was <0.04, whereas the maximum estimated viscous pressure gradient was approximately 5% of the hydrostatic gradient produced by the water. The maximum value of corresponding capillary number was 2.5E-6.

The experimental procedure provided uncertainties in the measured parameters that were deemed acceptable. The uncertainty in the porosity was estimated to be 0.005, based on the deviation of the values calculated from the two beams. The total (calibration plus measurement) uncertainty in the calculated liquid saturations was approximately 0.02.

A volume balance on the LNAPL was performed for each run by comparing the initial volume added to the amount present at the end of the run. The final volume was found by adding the volume of the free displaced layer to the volume in the test section found by integrating the Soltrol saturations. The initial and final volumes matched within 10% for all runs. The agreement is good, considering the error caused by using only six integration points over a 9-in. test section.

IV. DISCUSSION OF RESULTS

Experiments were performed using six sizes (210, 360, 710, 1500, 3000, and 6000 μm) of glass particles and a standard test soil known as Synthetic Soil Matrix® (SSM). The SSM and associated physical data were obtained from Foster Wheeler Enviresponse, Inc., a U.S. Environmental Protection Agency (EPA) facility in Edison, New Jersey. Based on fluid densities, measured gravimetrically, and interfacial tension, measured by the falling drop method, the Bond numbers corresponding to the six diameters of the glass particles were calculated and are shown in Table 2.

The method of packing the porous material provided fairly consistent porosities throughout the column and from run to run. The porosities calculated from Equation 3 for the glass particles ranged from 37 to 41%, whereas values for the SSM varied from 32 to 37%.

The measurement locations along the column were identified by the letters A through F (see Table 1 for locations). The initial water saturation profile was such that points A and B had a high saturation near 100%, E and F were dry, and C and D had an intermediate saturation. Due to difficulty in precisely repeating the initial water profile, the amount of LNAPL that penetrated to points A and B tended to vary from run to run, leading to some inconsistency in the LNAPL saturations at these locations.

Figure 6 summarizes the results using 360-μm particles. Figure 6A shows the initial water profile that was established, which varied from almost completely saturated at point A (2.7 in.) to completely dry at points E and F (6.5 and 7.2 in.). When the LNAPL was added (Figure 6B), there was a minimal impact on the water profile and the LNAPL filled most of the air space in the upper portion of the column. Figure 6c shows the saturation profiles after the water level was raised and the free LNAPL was displaced from the test section. There are two identifiable levels of residual saturation, corresponding to the portions of the column that were initially water-wet and water-dry.

TABLE 2
Test Bond Numbers

Particle diameter (μm)	Bond number
210	0.00222
360	0.00651
710	0.0253
1500	0.113
3000	0.452
6000	1.81

Figures 6d and 6e show the second cycle of the water level being lowered and raised. The free LNAPL previously displaced is allowed to reenter the column during the water drainage phase. When the water level is raised again, the distribution of the LNAPL (Figure 6E) is quite even and reflects similar behavior to the water-wet regions of the column during the first displacement.

Figure 7 shows the same series of measurements for 210-μm particles. The behavior is similar to that on Figure 6. Figures 7D and 7E show that the LNAPL penetrated farther into the column than it had for the 360-μm run, due to slight inconsistencies in the amount of water drained between displacements from run to run.

The results for 710-μm particles are shown in Figure 8. Some expected effects of the particle diameter change are reflected in the initial water profile (Figure 8A) and the LNAPL profile after the water level is lowered (Figure 8D). Again, however, the distribution of LNAPL after the first and second displacements is essentially identical to the behavior with the other diameters.

The range of diameters from 210 to 710 μm spans the range found in medium sandy soils (Bear, 1972). The water-wet regions in the test section would seem to

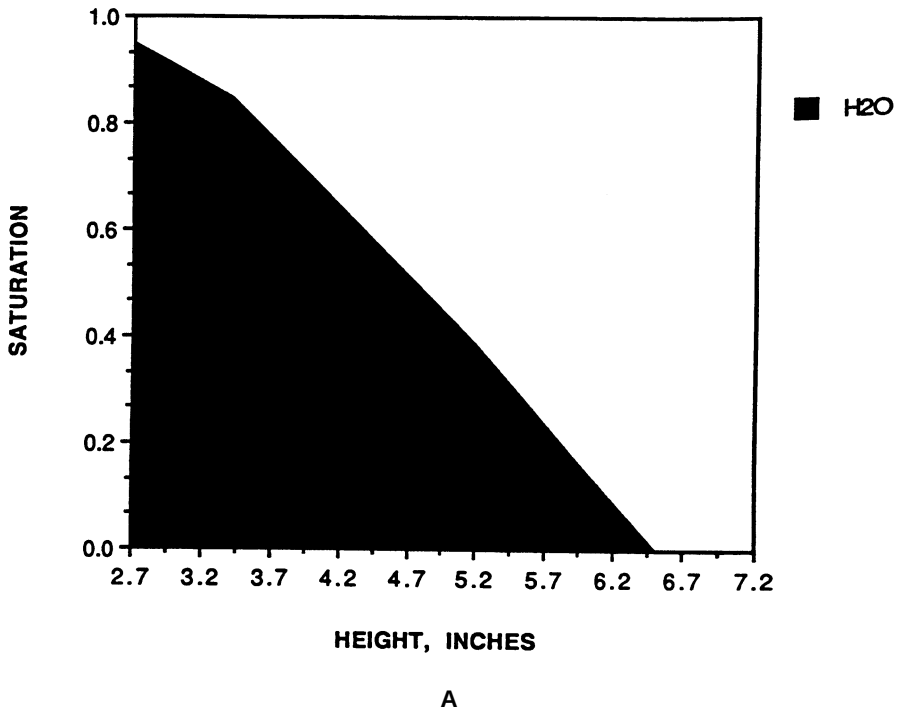

FIGURE 6. (A) Initial water saturation profile (360-μm particles). (B) Saturation profiles after LNAPL addition (360-μm particles). (C) Saturation profiles after first displacement by water (360-μm particles). (D) Saturation profiles after water table was lowered (360-μm particles). (E) Saturation profiles after second displacement by water (360-μm particles).

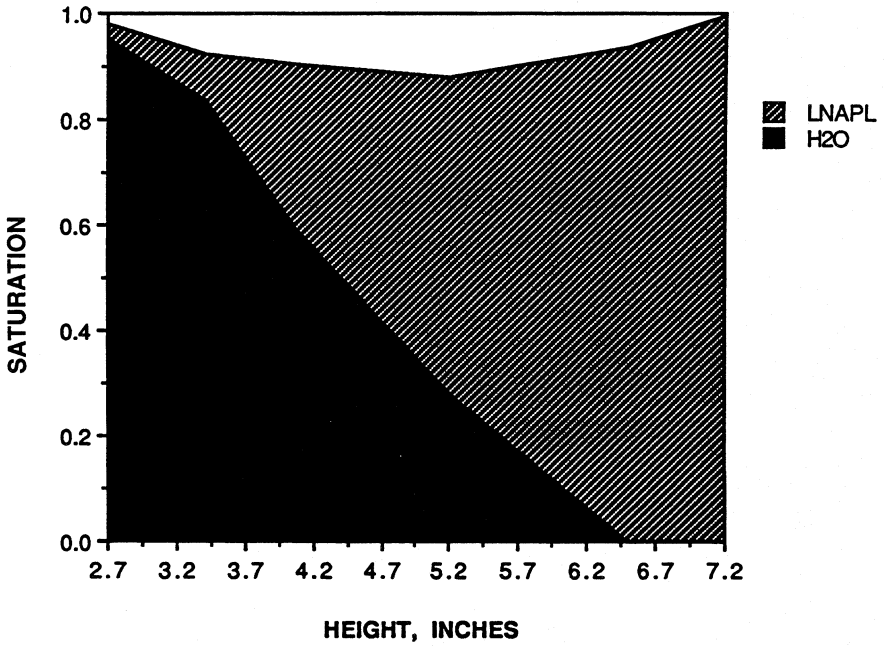

FIGURE 6B

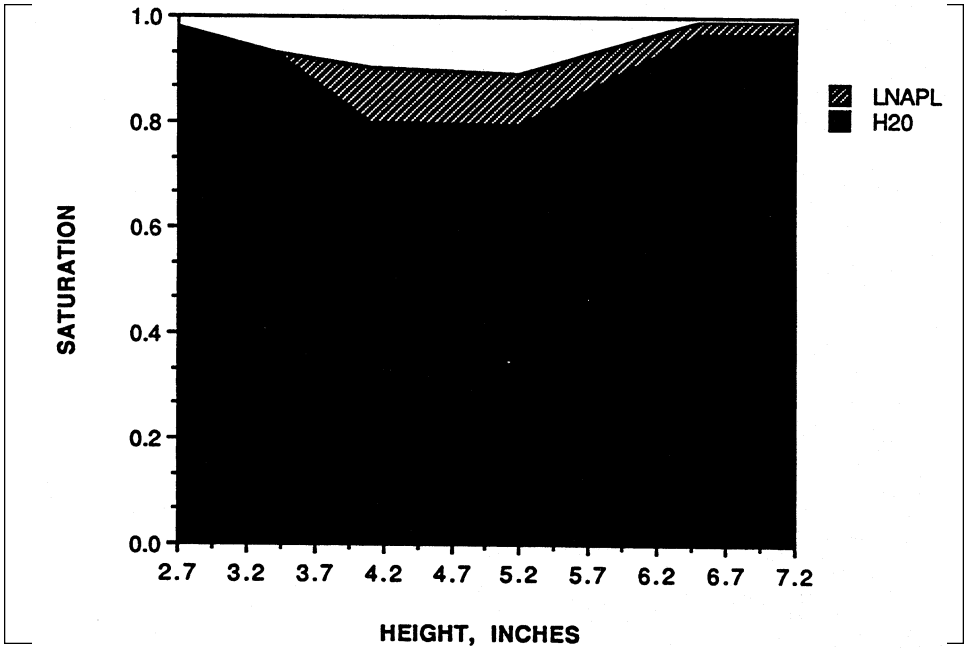

FIGURE 6C

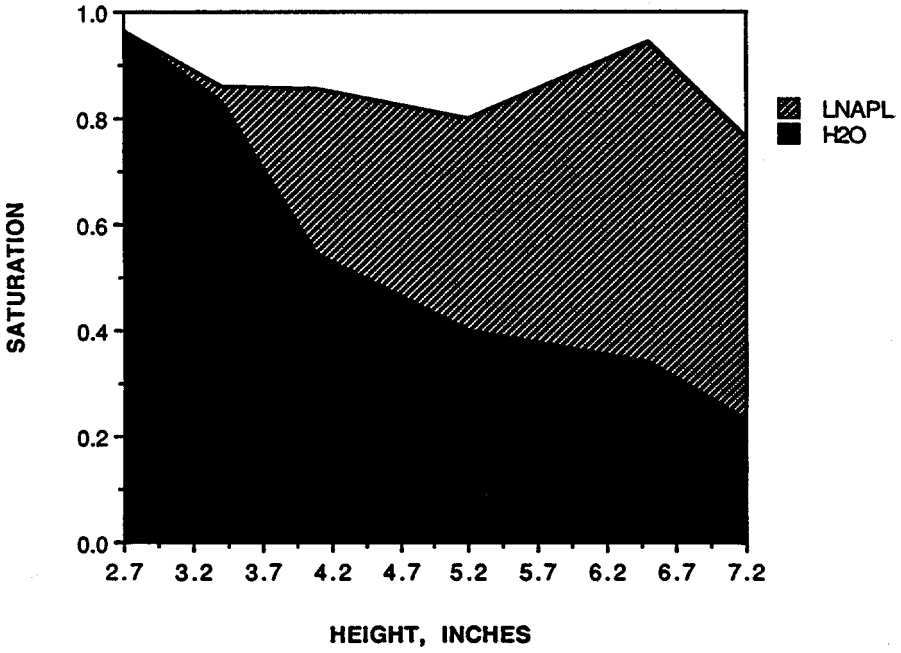

FIGURE 6D

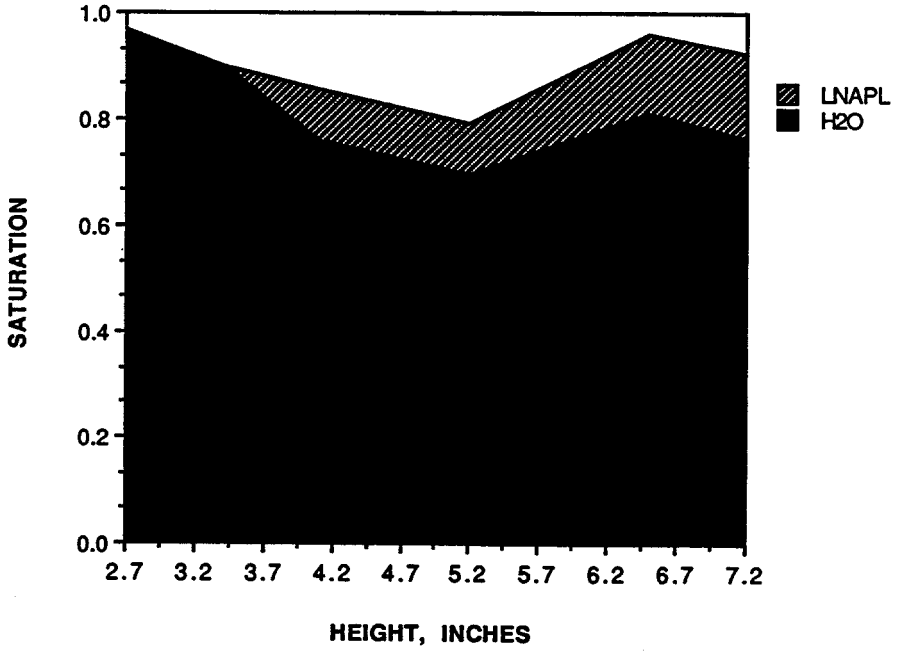

FIGURE 6E

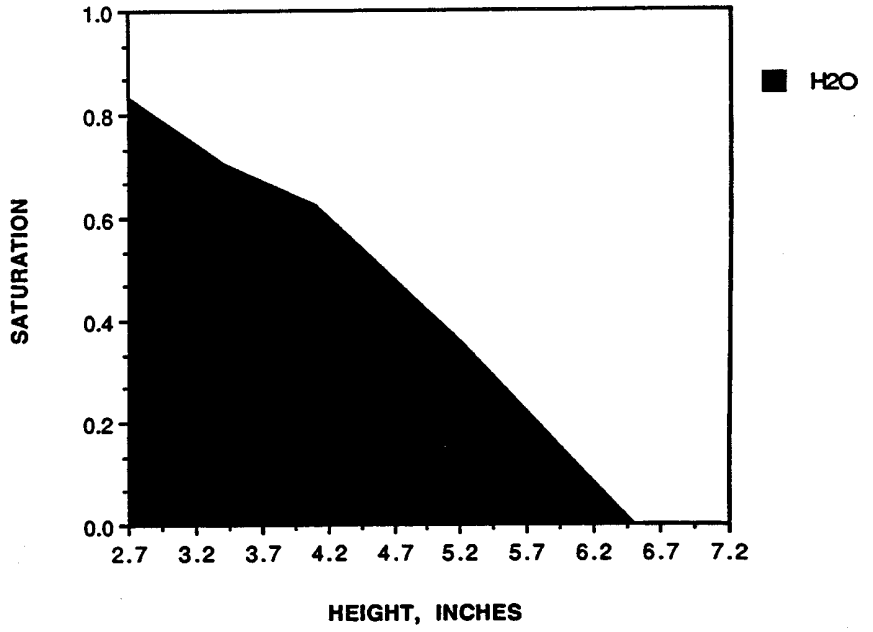

A

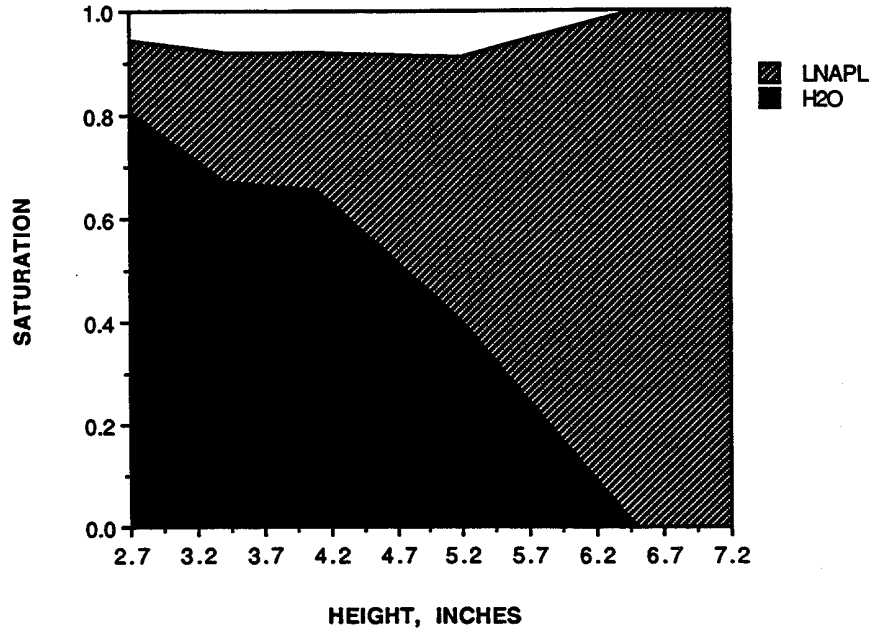

B

FIGURE 7. (A) Initial water saturation profile (210-μm particles). (B) Saturation profiles after LNAPL addition (210-μm particles). (C) Saturation profiles after first displacement by water (210-μm particles). (D) Saturation profiles after water level was lowered (210-μm particles). (E) Saturation profiles after second displacement by water (210-μm particles).

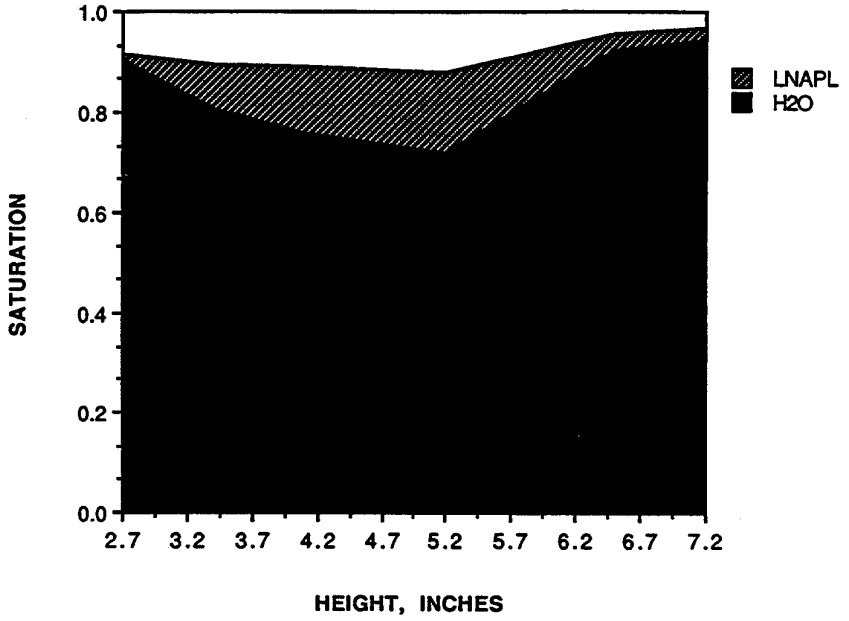

FIGURE 7C

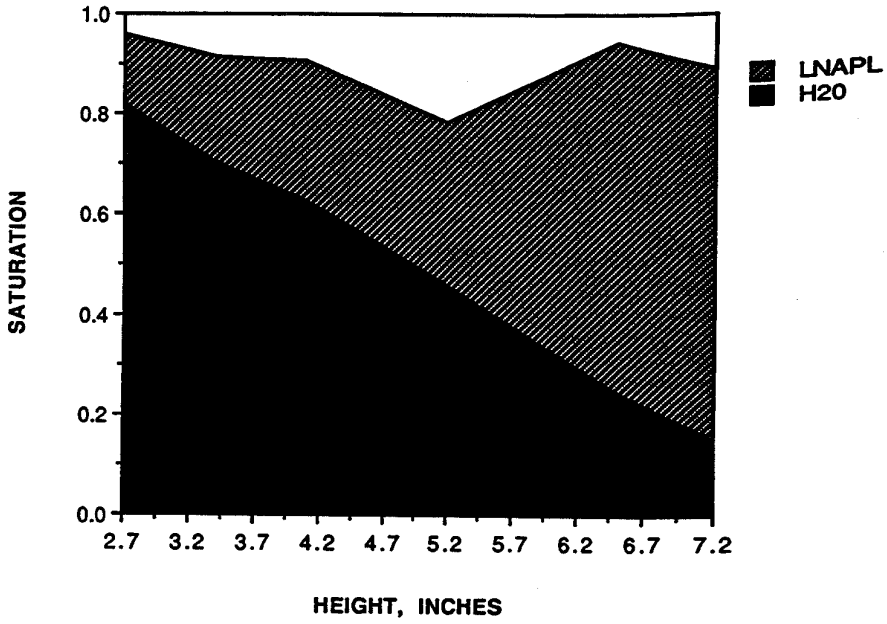

FIGURE 7D

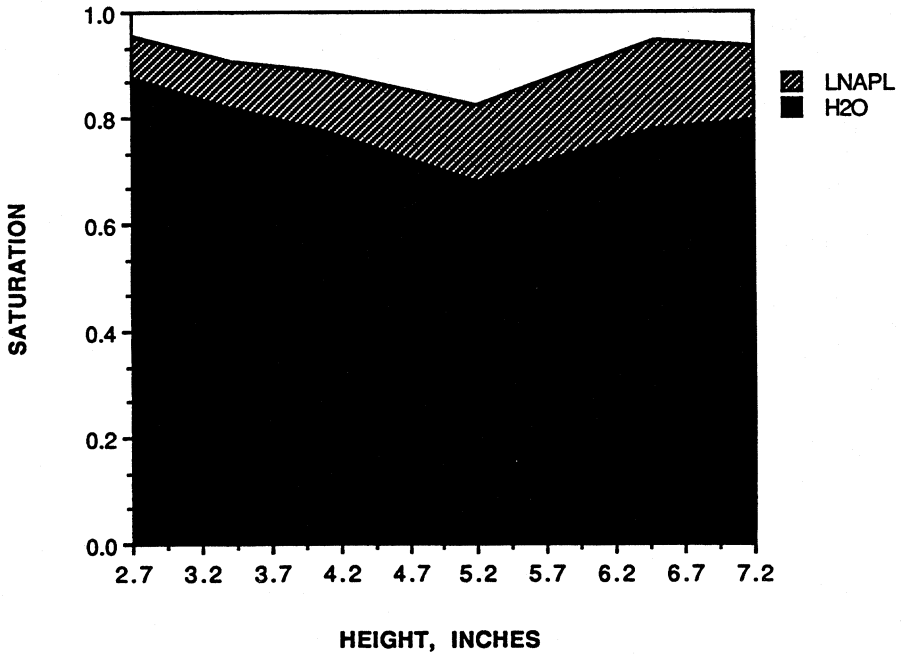

FIGURE 7E

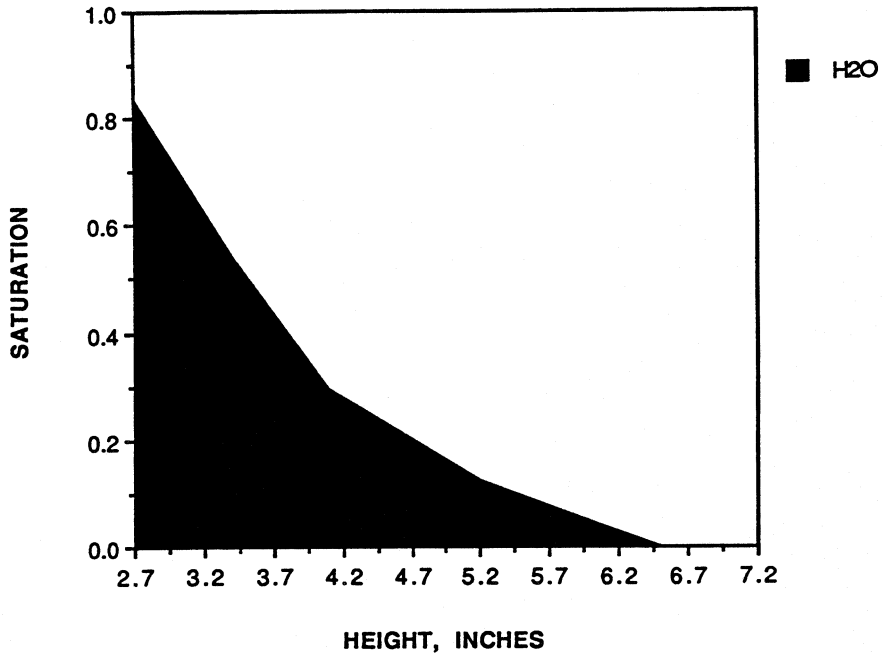

A

FIGURE 8. (A) Initial water saturation profile (710-μm particles). (B) Saturation profiles after LNAPL addition (710-μm particles). (C) Saturation profiles after first displacement by water (710-μm particles). (D) Saturation profiles after water level was lowered (710-μm particles). (E) Saturation profiles after second displacement by water (710-μm particles).

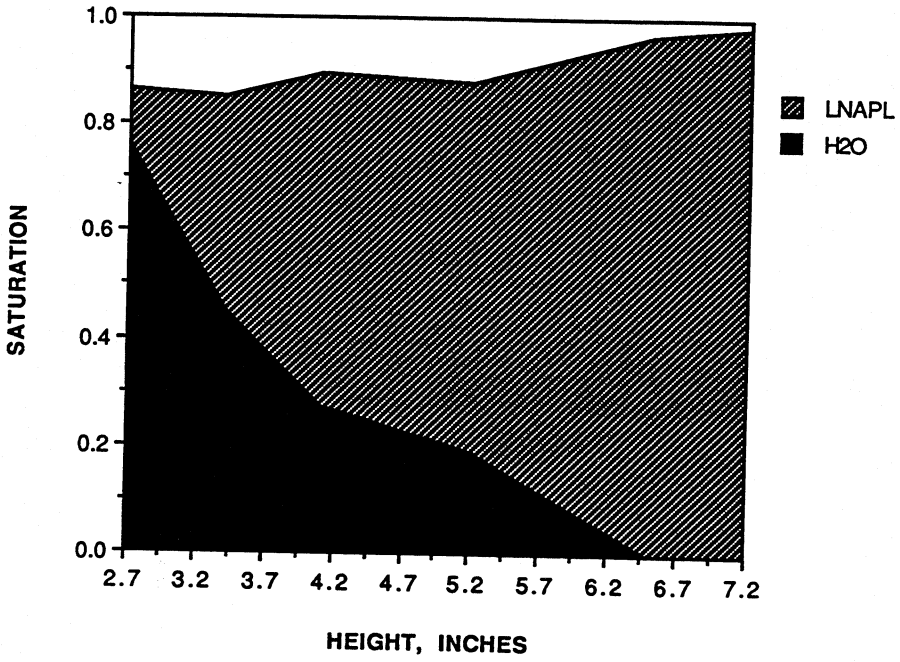

FIGURE 8B

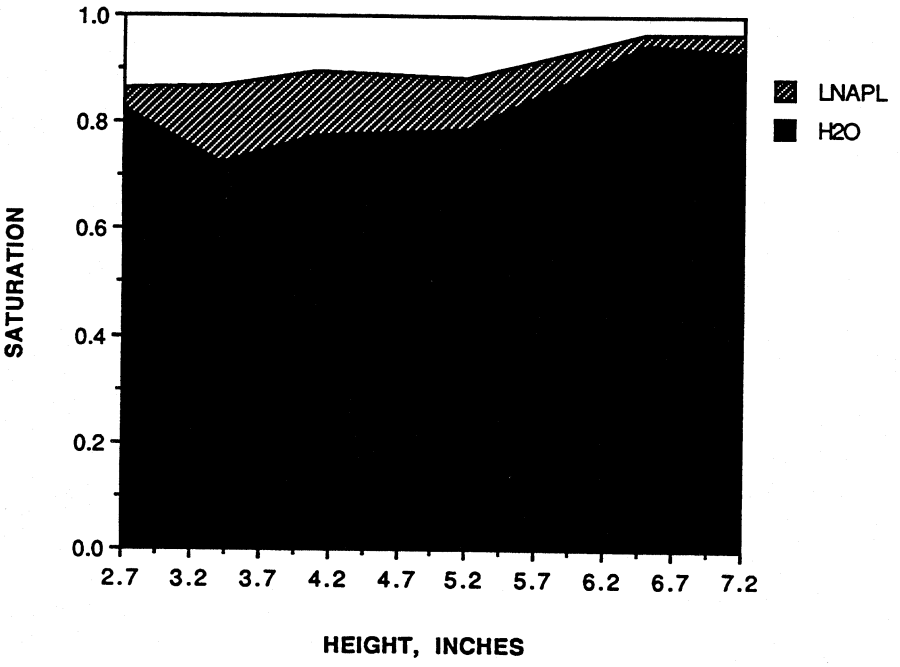

FIGURE 8C

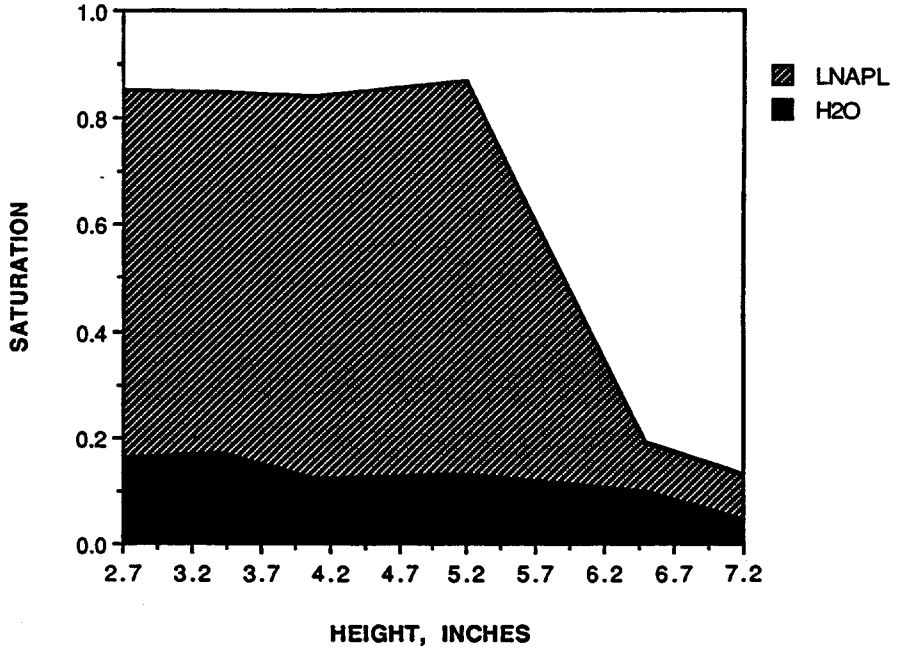

FIGURE 8D

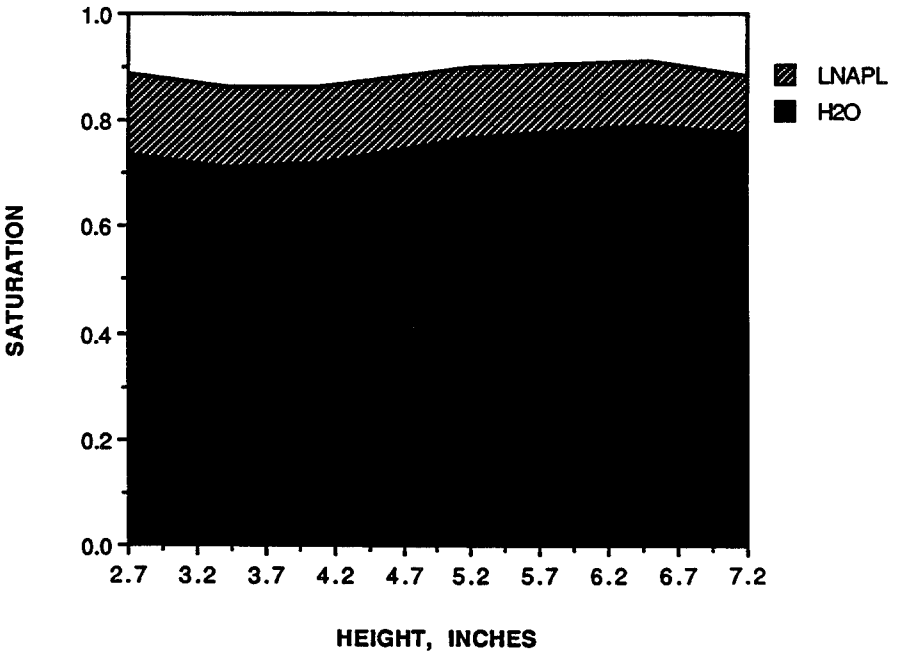

FIGURE 8E

be most representative of natural soil conditions near the water table. Over this diameter range, and for these test conditions, the residual LNAPL saturation averages 13%. It is interesting to note that the extent of the initial water saturation does not appear to influence the LNAPL residual saturation, except when the initial water saturation is fairly high (>80%). At these initial water conditions, there is a negligible amount of LNAPL trapping. The effect of a large initial water saturation can be seen in Figures 6B and 6C, Figures 6D and 6E, and Figures 7B and 7C. This behavior implies that the largest pores may not be conducive to trapping. The insensitive relationship between LNAPL residual saturation and lower initial water saturation values indicates that there is a medium range of pore sizes that are most likely to trap LNAPL.

The small values of residual saturation in the water-dry portions of the test section reflect the different contact angle that exists in this region. According to the estimates of Oh and Slattery (1979), there is a somewhat higher pressure difference required to mobilize ganglia under oil-wet conditions, which would indicate a tendency for higher residual saturations. The lower residual saturation in the water-dry regions appears to be due to the effect of contact angle on the trapping process. It is probable that the entrapped LNAPL in the water-dry regions is in the form of pendular rings at the contact points between particles rather than ganglia filling the belly of the pores, leading to the lower saturation values. It is somewhat difficult to quantify accurately the residual saturation in this region because the saturation value is nearly the same as the inherent measurement uncertainty in the gamma densitometer method. In general, though, the similarity in Figures 6, 7, and 8 provides good confidence in the experimental values.

Effort was made to determine the effect of the specific test conditions on the results, particularly the reintroduction of the displaced LNAPL to the test section as the water level was lowered. This part of the procedure was meant to represent a large spill in which there is a surplus of free LNAPL above the capillary fringe. To simulate conditions in which the spill is smaller or has had more opportunity to disperse laterally, a special test was run using 360-μm particles. The test procedure was the same, except that the free LNAPL removed after the first displacement was removed from the test apparatus before the water level was lowered. In addition, the water level was lowered a second time, and a third displacement was performed with the goal of assessing how a finite amount of residual LNAPL would redistribute after several water table oscillations.

The results for this run are shown in Figure 9. Note that an anomaly in the initial water profile appears at a height of 4.1 in., which would seem to indicate a heterogeneity in packing, although no corresponding variation in porosity was detected. Despite this anomaly, there is no discernible effect on residual LNAPL saturations. The LNAPL distribution after the first displacement is similar to those shown previously. Comparing Figures 9D and 9E (second displacement) to Figure 9F and 9G (third displacement), it is apparent that the water level was lowered more before the third displacement, causing the LNAPL to migrate further into the

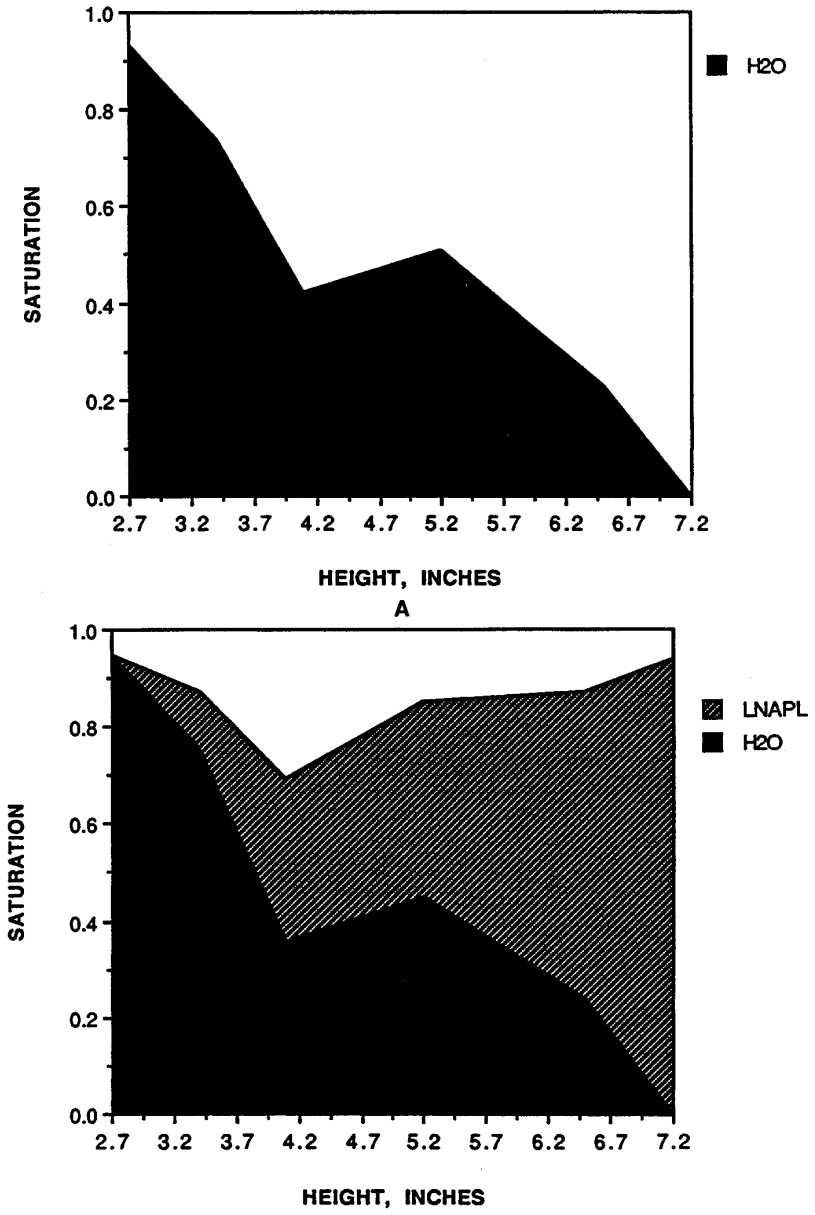

FIGURE 9. (A) Initial water saturation profile (360-μm particles, special run). (B) Saturation profiles after LNAPL addition (360-μm particles, special run). (C) Saturation profiles after first displacement by water (360-μm particles, special run). (D) Saturation profiles after water level was lowered the first time (360-μm particles, special run). (E) Saturation profiles after second displacement by water (360-μm particles, special run). (F) Saturation profiles after water level was lowered the second time. (360-μm particles, special run). (G) Saturation profiles after third displacement by water (360-μm particles, special run).

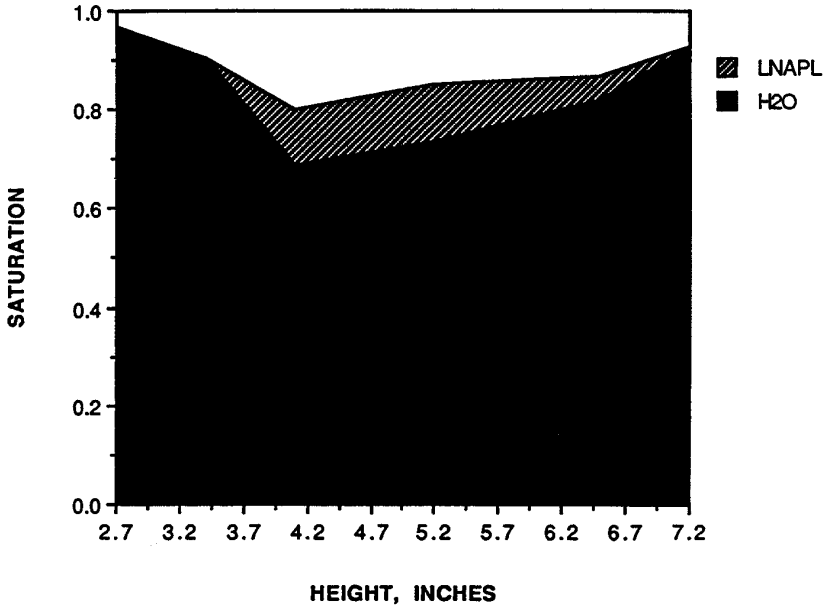

FIGURE 9C

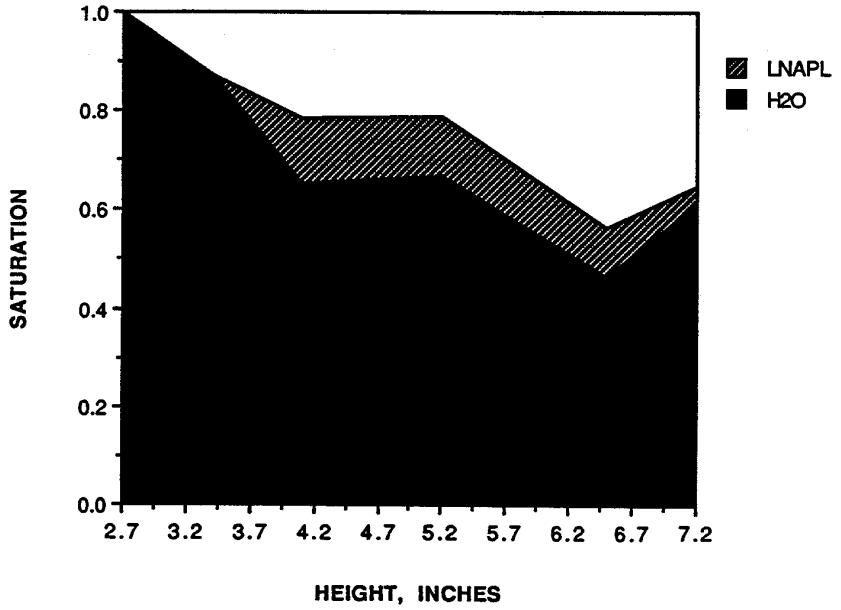

FIGURE 9D

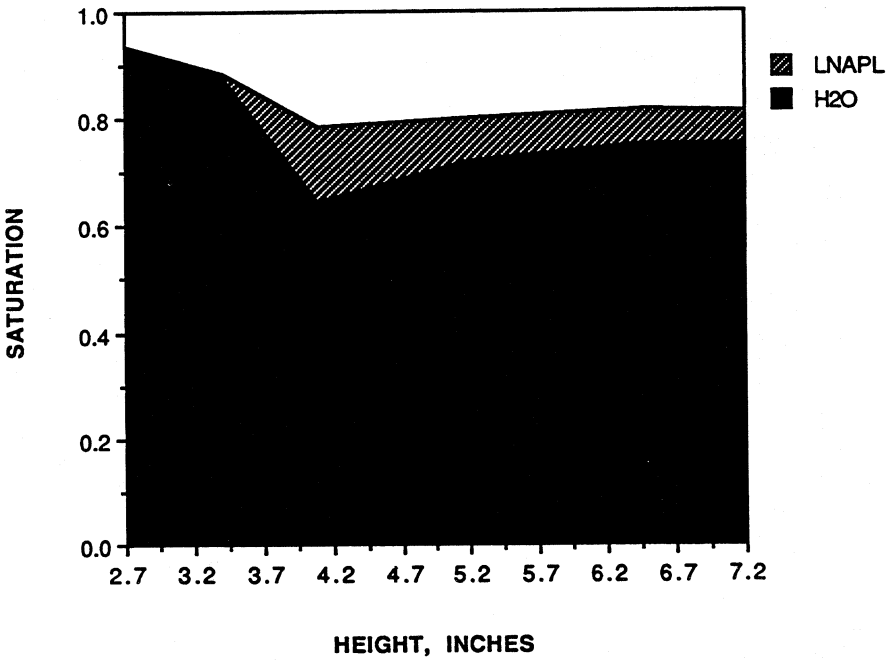

FIGURE 9E

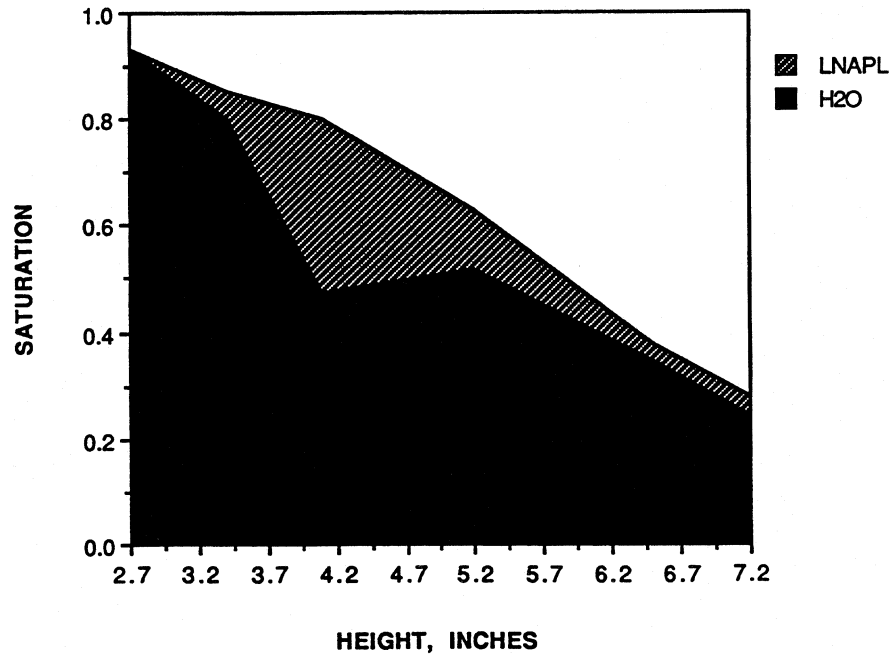

FIGURE 9F

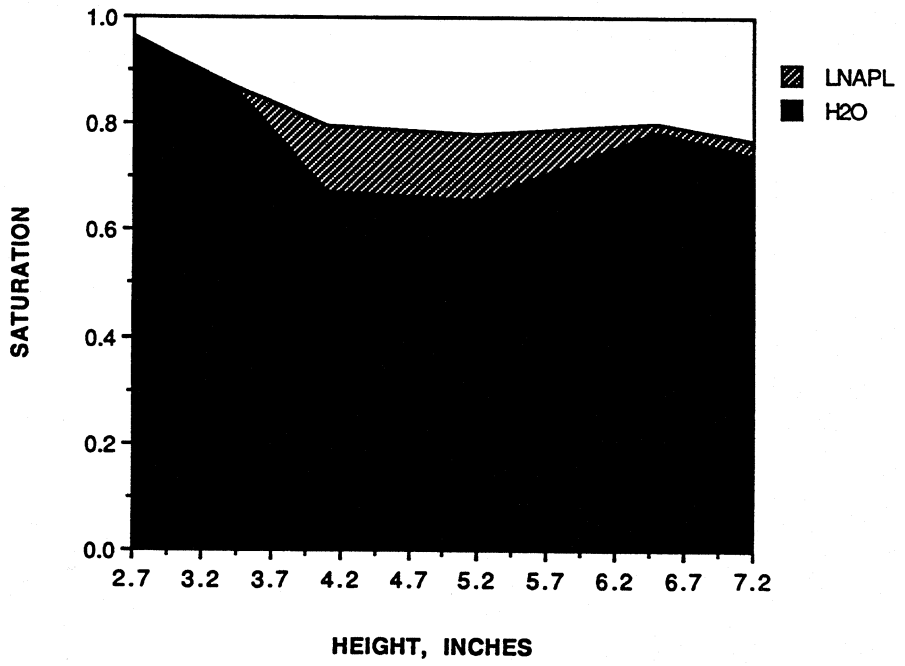

FIGURE 9G

lower portion of the test section. The result is a slightly larger residual saturation in the middle part of the test section after the third displacement, which reduces the LNAPL saturation in the upper part of the column due to the finite amount of LNAPL. It is apparent that differences in the pattern of water table oscillation can have some effect on how a fixed amount of trapped LNAPL is distributed.

Another variable that may have an effect on residual saturation is the particle-size distribution, which influences the pore-size distribution. The relationship between the particle-size and pore-size distributions has been noted in Lenhard and Parker (1990). To evaluate experimentally the effect of particle-size distribution and to test the validity of the glass bead data for actual soils, an experiment was run with the SSM, approved by the EPA for contamination studies. The particle-size distribution, provided by Foster Wheeler Enviresponse, Inc., is illustrated in Figure 10. The particle-size range of the SSM more than covers the range of the diameters used to acquire the results in Figures 6 through 9.

The SSM test used the same procedure as the runs shown in Figures 6, 7, and 8. The test results are shown in Figure 11. A significant effect of the particle- (or pore-) size distribution can be found in the initial water profile (Figure 11a). There is also a significant amount of trapped air after the addition of LNAPL (Figure 11b). Nevertheless, the amount of trapped LNAPL after the first and second water displacements compares well with the glass bead data. It should be noted that there

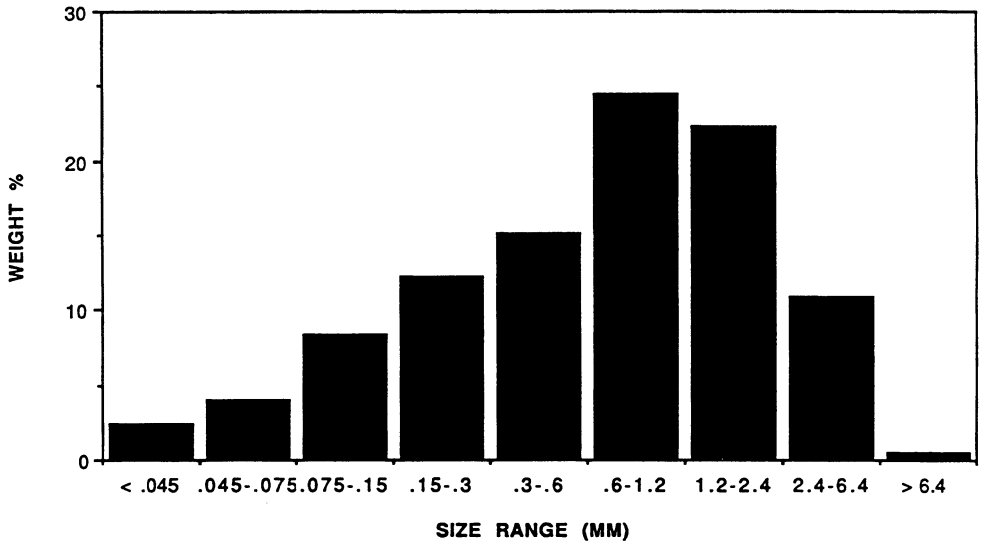

FIGURE 10. Size distribution of SSM (typical).

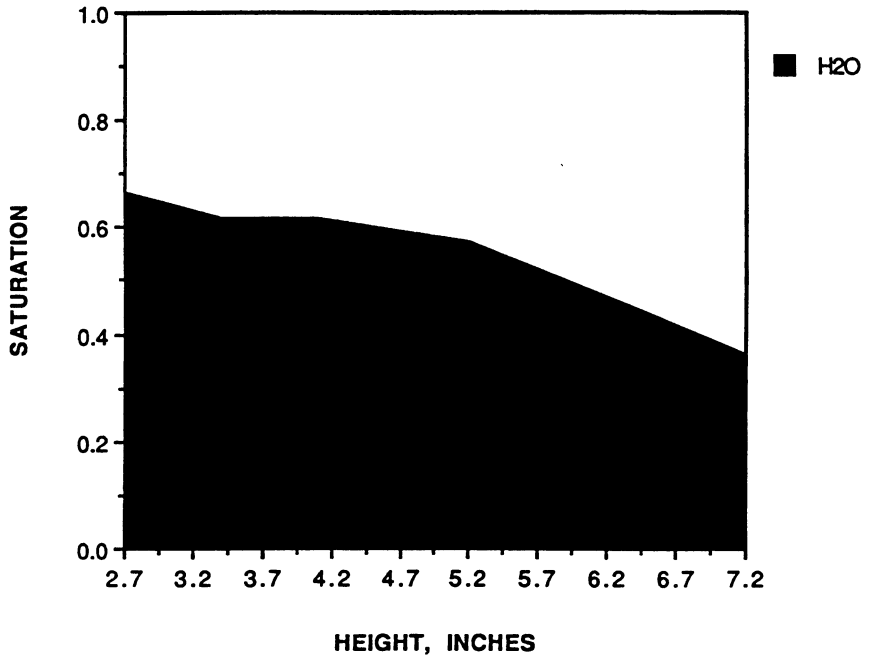

A

FIGURE 11. (A) Initial water saturation profile (SSM). (B) Saturation profiles after LNAPL addition (SSM). (C) Saturation profiles after first displacement by water (SSM). (D) Saturation profiles after water level was lowered (SSM). (E) Saturation profiles after second displacement by water (SSM).

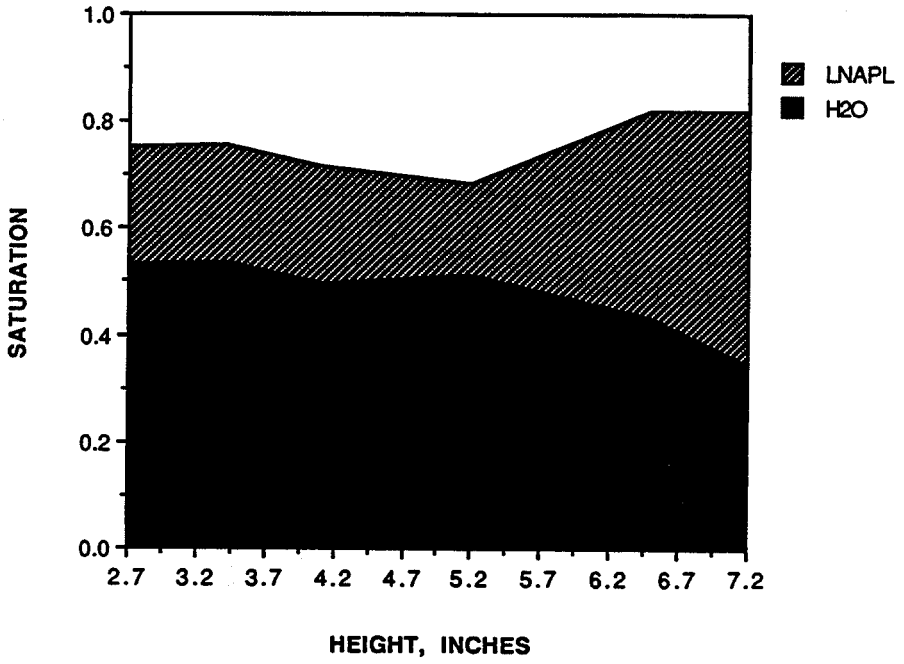

FIGURE 11B

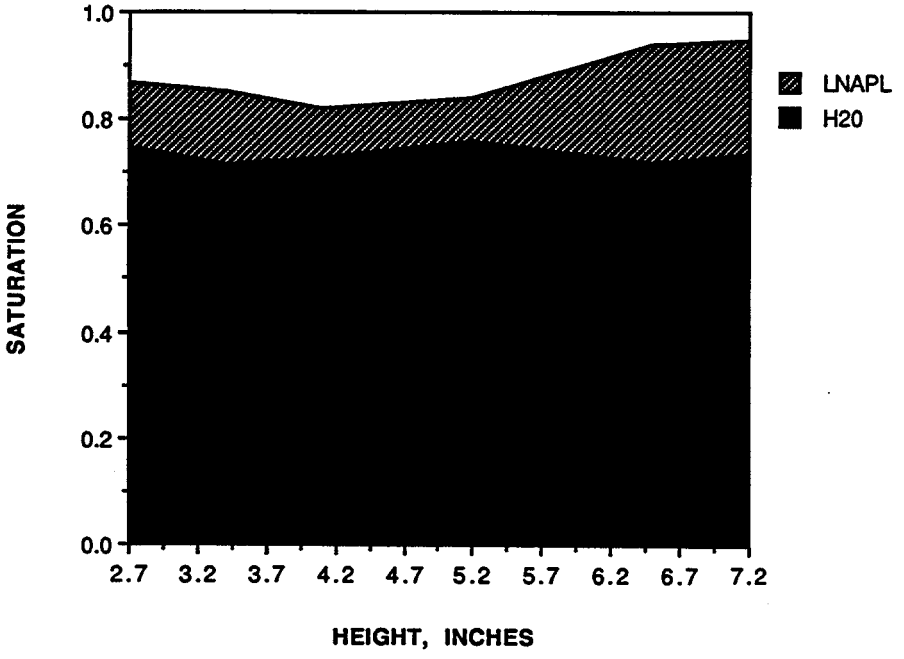

FIGURE 11C

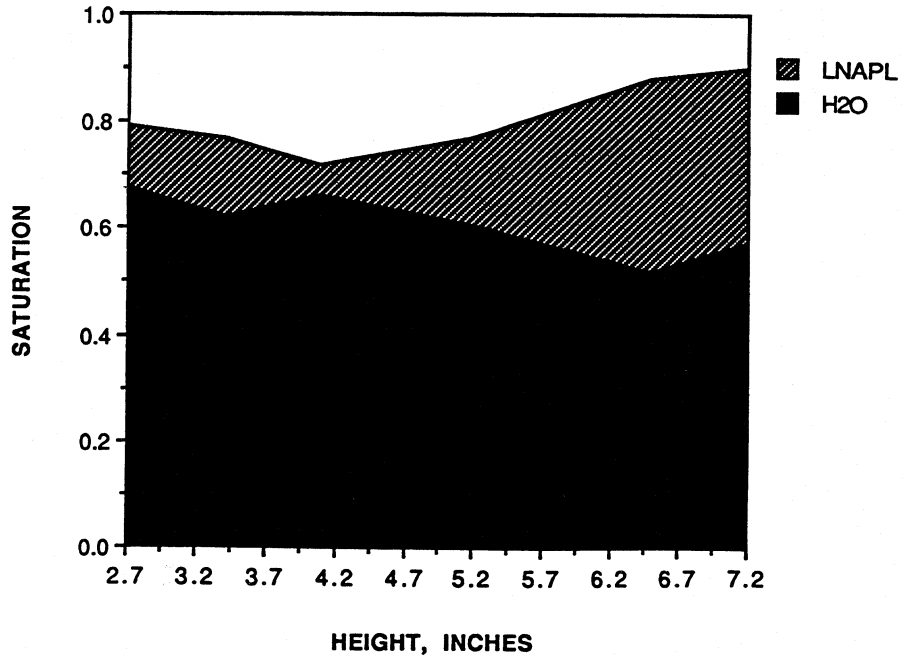

FIGURE 11D

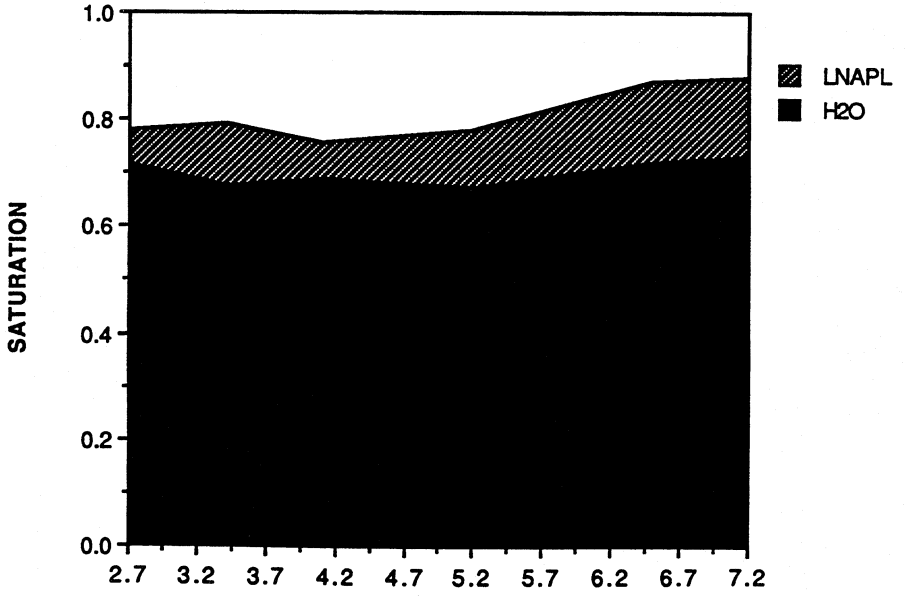

FIGURE 11E

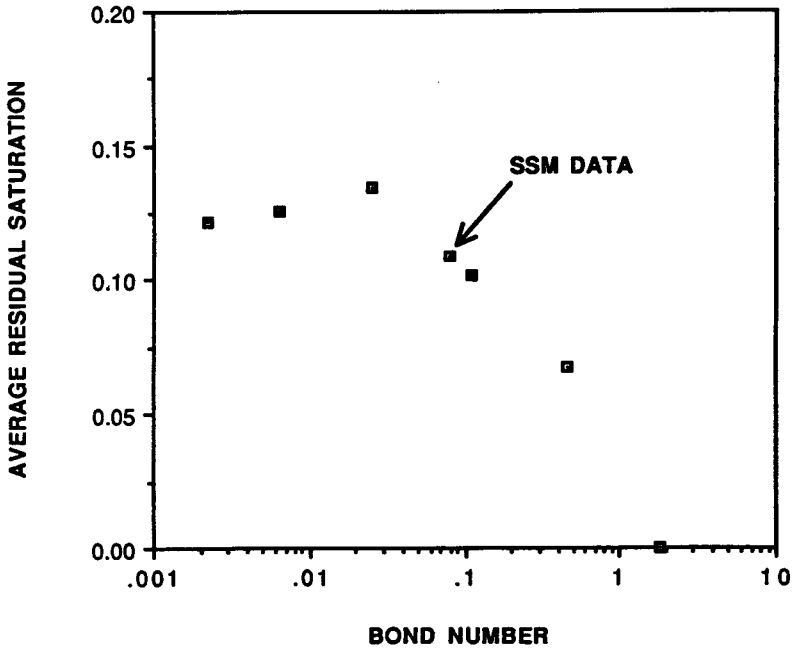

FIGURE 12. Effect of Bond number on residual saturation.

was no initially water-dry portion in this run due to the initial water profile that was achieved. There is some indication in Figure 11c that there may be a dependence between the LNAPL residual saturation and the initial level of water saturation. However, the LNAPL distribution for the second displacement shown in Figure 11e compares very well with the glass bead data. Comparing the results for the SSM and glass beads, there is a remarkable similarity in the residual LNAPL saturation profiles, considering the differences in particle-size distribution and material type. It should be mentioned that the possibility of soil swelling occurs when using natural materials such as the SSM, which would introduce an experimental error in the dual-beam gamma densitometer technique (which assumes a nonswelling medium); however, there is nothing in the results that indicates this was a problem.

It is somewhat difficult to compare these results with other published data due to the differences in initial conditions and test procedures. Most of the previous work related to residual hydrocarbon saturation in the subsurface has focused on the vadose zone. For example, Hoag and Marley (1986) measured the residual saturation of gasoline under drainage conditions for sandy soils of various particle diameters. Dry soils and soils at field capacity moisture content were used. Values of residual saturation as high as 60% were found for dry, fine soils, but the initial moisture content had a significant effect on the results. For the initially moist,

medium sands, the average residual saturation of gasoline was 15%, which is in reasonable agreement with the results shown here. Values of 16 to 18% for residual saturation for several fluids under drainage conditions in glass beads were found by Moseley and Dhir (1992).

Lenhard *et al.* (1989) published numerical simulations of the entrapment of an "oil slug" due to an oscillating water table. The value of the NAPL specific gravity used in the simulations was 0.8. The calculated saturation distribution of trapped LNAPL showed a strong dependence on initial water content that is not consistent with the results obtained here. The maximum value of trapped LNAPL saturation was calculated to be about 20%.

To evaluate the existence of a critical Bond number, similar tests were conducted for larger particle diameters (1500, 3000, and 6000 μm). Because the LNAPL saturation values after the second water displacement were deemed to be most representative of aquifer conditions (i.e., the whole test section was water-wet), these results were used to assess the effect of particle diameter. The average LNAPL saturation for each particle diameter was calculated and compared to the corresponding Bond number. This relationship is shown in Figure 12. The SSM results are included as well by basing the Bond number on the average particle diameter. As the order of the Bond number approaches one, the residual saturation begins a gradual decline. At the Bond number of 1.8, corresponding to a particle diameter of 6000 μm, the residual saturation has dropped to undetectable levels.

The experimental value of critical Bond number agrees well with the predicted value of 1.6 found by analogy with the critical capillary number of 1E-3. The predicted values based on the periodically constricted tube model of Oh and Slattery (1979) are too high by an order of magnitude. The difference is probably due to the geometric model, but the results are still valuable in predicting the effect of pore size and contact angle on the required mobilization pressure difference.

The existence of a critical Bond number allows an estimate of the reduction in interfacial tension that is required to facilitate the displacement of entrapped LNAPL for a given particle diameter. For example, using the densities for the fluids used in these experiments and a particle diameter of 360 μm, the interfacial tension required to give a Bond number of 1.6 is 0.24 dyn/cm. Interfacial tensions as low as 0.1 dyn/cm for a water/isopropyl alcohol/isooctane system in the laboratory have been reported by Morrow et al. (1988); the achievement of these values in the field has not been demonstrated.

V. SUMMARY AND CONCLUSIONS

A dual-beam gamma densitometer was used successfully to measure residual LNAPL saturations after displacement by an oscillating water table. The tests were performed in a 3-in.-diameter column using glass beads and a standard soil as the porous media. Most of the experiments were run with an excess amount of free

LNAPL above the capillary fringe so that the maximum level of LNAPL entrapment could be evaluated.

For particle diameters representative of medium sandy soils, the residual saturation of entrapped contaminant averaged 13%. The distribution of contaminant was quite even as long as the medium was initially water-wet. There was no discernible effect of the amount of initial moisture present, except at initial water saturations above 80%. Results from a test using a finite amount of LNAPL showed that the distribution of entrapped LNAPL is somewhat dependent on the amount that the water table is lowered between upward displacements.

Residual saturations in the water-dry portions of the test section were much lower than anticipated. It is apparent that the contact angle of the medium has a pronounced effect on the LNAPL trapping process. The low residual saturations probably reflect LNAPL in the form of pendular rings rather than ganglia trapped in the belly of the pores.

Experimental results with a representative soil were quite similar to the glass bead results, despite the large difference in particle-size distribution. The agreement between results with media of different types ensures that the results can be applied to the field with reasonable confidence.

Data from various particle sizes indicated that there was little effect of particle size up to 710 μm or a Bond number of 0.025. For larger particle diameters, the residual saturation decreased, reaching a negligible value at a Bond number of 1.8. This agrees well with the predicted critical Bond number of 1.6, based on the comparison with the critical capillary number of 1E-3. This agreement indicates that the mechanism of displacement by hydrostatic pressure gradients is analogous to displacement by viscous pressure gradients.

The experimental results provide a basis for estimating the amount of LNAPL trapped in the saturated zone, provided that the water table height is monitored after the spill reaches the capillary fringe. The value of the critical Bond number allows estimates of the reduction in interfacial tension required to remove the entrapped contaminant from the saturated zone by buoyancy forces alone.

REFERENCES

Baehr, A. L. 1987. Selective transport of hydrocarbons in the unsaturated zone due to aqueous and vapor phase partitioning. *Water Resour. Res.* **23**,

Bear, J. 1972. *Dynamics of Fluids in Porous Media.* New York, American Elsevier.

Boyd, G. R. and Farley, K. J. 1992. NAPL removal from groundwater by alcohol flooding: laboratory studies and applications. In: *Hydrocarbon Contaminated Soils and Groundwater,* Vol 2. (Calabrese, E. J. and Kostecki, P. T., Eds.) Lewis.

Faust, C. R. 1985. Transport of immiscible fluids within and below the unsaturated zone: a numerical model. *Water Resour. Res.* **21**,

Ferguson, H. and Gardner, W. H. 1962. Water content measurement in soil columns by gamma ray absorption. *Soil Sci. Soc. Am. J.* **26**,

Ferrand, L. A., Milly, P. C. D., and Pinder, G. F. 1986. Dual-gamma attenuation for the determination of porous medium saturation with respect to three fluids. *Water Resour. Res.* **22**,

Hoag, G. E. and Marley, M. C. 1986. Gasoline residual saturation in unsaturated uniform aquifer materials. *J. Environ. Eng.* **112**,

Hoag, G. E., Marley, M. C., Cliff, B. L., and Nangeroni, P. 1991. Soil vapor extraction research developments. In: *Hydrocarbon Contaminated Soils and Groundwater,* Vol 1. (Kostecki, P. T. and Calabrese, E. J., Eds.) Lewis.

Hunt, J. R., Sitar, N., and Udell, K. S. 1988. Nonaqueous phase liquid transport and cleanup. I. Analysis of mechanisms. *Water Resour. Res.* **24**,

Imhoff, P. T., Jaffe, P. R., and Pinder, G. F. 1990. Dissolution of organic liquids in groundwater. In: *Environmental Engineering, Proc. 1990 Specialty Conf. of the Environmental Engineering Div.* (O'Melia, C. R., Ed.) American Society of Engineers.

Lenhard, R. J. and Parker, J. C. 1988. Experimental validation of extending two-phase relations to three-fluid phase systems for monotonic drainage paths. *Water Resour. Res.* **24**,

Lenhard, R. J., Dane, J. H., Parker, J. C., and Kaluarachchi, J. J. 1988. Measurement and simulation of one-dimensional transient three-phase flow for monotonic liquid drainage. *Water Resour. Res.* **24**,

Lenhard, R. J., Parker, J. C., and Kaluarachchi, J. J. 1989. A model for hysteretic constitutive relations governing multiphase flow. III. Refinements and numerical simulations. *Water Resour. Res.* **25**,

Lenhard, R. J. and Parker, J. C. 1990. Estimation of free hydrocarbon volume from fluid levels in monitoring wells. *Ground Water* **28**,

Leverett, M. C. 1941. Capillary behavior in porous solids. *Trans. Am. Inst. Min. Eng.* **142**,

Morrow, N. R., Chatzis, I., and Taber, J. J. 1988. Entrapment and mobilization of residual oil in bead packs. *Soc. Pet. Eng. J. (Res. Eng.)* **3**,

Moseley, W. and Dhir, V. K. 1992. Capillarity in porous media and the Effect of Wettability. M.S. thesis. University of California, Los Angeles.

Nofziger, D. L. and Swartzendruber, D. 1974. Material content of binary physical mixtures as measured with a dual-energy beam of gamma rays. *J. Appl. Phys.* **45**,

Oh, S. G. and Slattery, J. C. 1979. Interfacial tension required for significant displacement of residual oil. *Soc. Pet. Eng. J.*

Parker, J. C. and Lenhard, R. J. 1987. A model for hysteretic constitutive relations governing multiphase flow. I. Saturation-pressure relations. *Water Resour. Res.* **23**,

Wardlaw, N. C. and McKellar, M. 1985. Oil blob populations and mobilization of trapped oil in unconsolidated packs. *Can. J. Chem. Eng.* **63**,